Ibid - Caltech Library System

Electronic Delivery Cover Sheet

Dynamic crack deflection and penetration at interfaces in homogeneous materials: experimental studies and model predictions

L. Roy Xu[a], Yonggang Y. Huang[b], Ares J. Rosakis[c,*]

[a] *Department of Civil and Environmental Engineering, Vanderbilt University, Station B 351831, Nashville, TN 37235, USA*
[b] *Department of Mechanical and Industrial Engineering, University of Illinois at Urbana-Champaign, Urbana, IL 16801, USA*
[c] *Graduate Aeronautical Laboratories, California Institute of Technology, Mail Stop 105-50, Pasadena, CA 91125, USA*

Abstract

We examine the deflection/penetration behavior of dynamic mode-I cracks propagating at various speeds towards inclined weak planes/interfaces of various strengths in otherwise homogeneous isotropic plates. A dynamic wedge-loading mechanism is used to control the incoming crack speeds, and high-speed photography and dynamic photoelasticity are used to observe, in real-time, the failure mode transition mechanism at the interfaces. Simple dynamic fracture mechanics concepts used in conjunction with a postulated energy criterion are applied to examine the crack deflection/penetration behavior and, for the case of interfacial deflection, to predict the crack tip speed of the deflected crack. It is found that if the interfacial angle and strength are such as to trap an incident dynamic mode-I crack within the interface, a failure mode transition occurs. This transition is characterized by a distinct, observable and predicted speed jump as well as a dramatic crack speed increase as the crack transitions from a purely mode-I crack to an unstable mixed-mode interfacial crack.

* Corresponding author. Tel.: +1-626-395-4523; fax: +1-626-449-6359.
 E-mail address: rosakis@aero.caltech.edu (A.J. Rosakis).

1. Introduction

When cracks propagate in homogeneous, brittle solids, they can only do so under locally mode-I conditions and at sub-Rayleigh wave speeds typically below the crack branching speed (Freund,1990; Broberg, 1999). Indeed, even if the applied far-field loading is asymmetric, the dynamically growing crack will curve and follow the path that will result to locally opening (mode-I) conditions at its tip making mix-mode and pure mode-II crack growth in homogeneous materials a physical impossibility. In addition, as the crack accelerates, under increasing far-field loading, it reaches a critical speed beyond which it becomes energetically more favorable to propagate with multiple, branched crack tips rather than as a single entity. This is called the branching speed which for a material like Homalite-100 is approximately equal to $0.35c_S$.

The situation is entirely different if a crack is constrained to propagate along a weak preferable path in an otherwise homogeneous solid. In this case and depending on the bond strength, the weak crack path or bond often traps the crack, suppresses any tendency of branching or kinking out of the weak plane and permits very fast crack growth much beyond the speeds observable in monolithic solids (Rosakis et al., 1999). Indeed, when mode-I cracks propagate in both isotropic and orthotropic solids containing weak crack paths (Washabaugh and Knauss, 1994; Coker and Rosakis, 2002), they can reach speeds as high as the Rayleigh wave speed of the solid. On the other hand, when mode-II cracks are made to propagate along such weak cracks, they tend to go even faster with speeds that are clearly within the intersonic regime of the solid (Rosakis et al., 1999; Gao et al., 1999; Geubelle and Kubair, 2001; Coker and Rosakis, 2002).

Although the extreme mode-I and mode-II cases have recently been studied experimentally and theoretically, very little is known about the dynamic mixed-mode crack growth along weak paths, a situation that has only recently been analyzed by Geubelle and Kubair (2001), and about the transition of an incident dynamic mode-I crack into a mixed-mode crack as it encounters a weak plane or interface. In the present work, we examine the incidence of dynamically growing cracks at inclined interfaces of various strengths. Our first goal is to observe this phenomenon experimentally and to establish and validate a dynamic deflection/penetration criterion. We then concentrate on the deflection behavior and examine mixed-mode crack growth along an interface.

It should be noted that static deflection/penetration behavior at an interface has been the subject of numerous research efforts in the past years and that many significant results for various kinds of materials have been obtained (Cook and Gordon, 1964; He and Hutchinson, 1989; Gupta et al., 1992; Evans and Zok, 1994; Martinez and Gupta, 1994; Ahn et al., 1998; Leguillon et al., 2000; He et al., 2000; Qin and Zhang, 2000). For quasi-statically growing cracks, the fracture toughness ratio of the interface and the matrix material has been identified as the most important parameter governing the crack deflection/penetration phenomenon and has formed the basis of a highly successful crack deflection/penetration criterion (Hutchinson and Suo, 1992). To authors' knowledge and with very few notable exceptions (Siegmund et al., 1997), the equivalent dynamic problem has remained unexplored. In this paper we deal only with an important subset of this problem. In particular, we consider weakly bonded systems
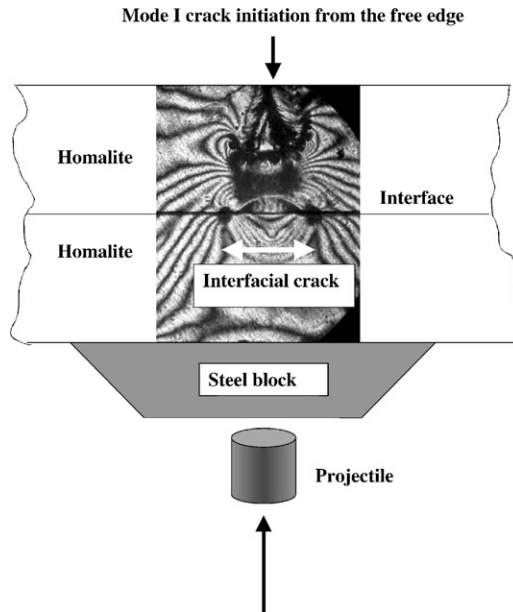
Fig. 1. Experimental evidence of the dynamic equivalent of the "Cook–Gordon mechanism". A fan of mode-I cracks is incident on a horizontal interface inducing intersonic debonding before these mode-I cracks reach the interface (Xu and Rosakis, 2002a).

composed of identical constituent solids so that the resulting material remains constitutively homogeneous. However, the existence of a weak bond (bond of lower fracture toughness) makes this material inhomogeneous regarding its fracture resistance behavior. By doing so we avoid the complication of the material property and wave speed mismatch across the interface, while retaining the essential properties of a weak path or bond whose strength can be experimentally varied and analytically modeled.

Motivation for studying this basic problem comes from our recent experimental observations of dynamic failure mechanisms in bonded Homalite layers subjected to projectile impact (Xu and Rosakis, 2002a). A visual example of the interaction of a fan of dynamically moving mode-I branches incident on a weak interface is shown in Fig. 1 (dynamic equivalent of the Cook–Gordon mechanism). The horizontal line in this picture represents an interface between two weakly bonded Homalite layers. As the subsonic mode-I cracks approach the interface, one central shear-dominated interfacial crack is nucleated and propagates along the bond at intersonic speeds providing an illustrative example of failure mode transition. This nucleation and growth of a symmetrically growing intersonic shear crack along a straight-line path is extensively discussed in the book by Broberg (1999). Fig. 1 is the direct evidence that such cracks exist and may be nucleated through remote interaction of incoming mode-I cracks with weak interfaces. Another example of the interaction between mode-I crack growth and an interface is given in the post-mortem picture of Fig. 2(a). Here two mode-I branches are incident onto the same vertical interface at approximately the same speed. The two
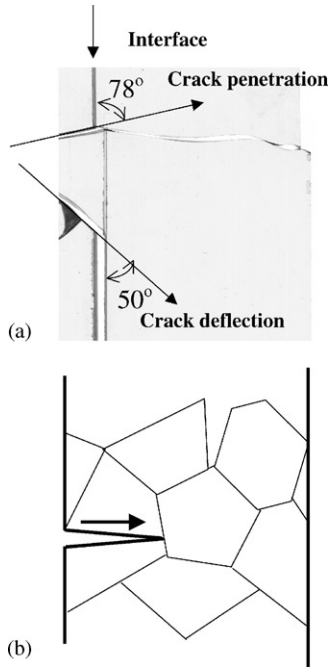
Fig. 2. Examples of the dynamic crack deflection/penetration at an interface. Case (a): In a layered Homalite material, the incident cracks traveled at 300 m/s. If the angle between the crack path and the interface is small, the dynamic crack cannot penetrate the interface and only causes interface debonding (Xu and Rosakis, 2002a). Case (b): Dynamic crack propagation towards a grain boundary.

cracks meet the interface at two different incident angles (angle between the crack path and the interface). As evident form the picture, the crack that meets the interface at 78° penetrates the interface while the other one is trapped by it (incident angle is 50°). Another motivation comes from the question of dynamic crack propagation in brittle heterogeneous solids (composed of large grains bonded together by weak grain boundaries). Examples of such solids include marble (Rosakis, 2000) or certain classes of high explosives (Dienes, 1996). Fig. 2(b) shows a dynamic crack propagating towards a grain boundary, which it may penetrate or follow depending on the incident crack speed, incident crack angle as well as the relative toughnesses between the grain and the grain boundary.

2. Experimental procedures

2.1. Materials and specimens

Similar to previous dynamic experiments (Rosakis et al., 1998), Homalite-100 was selected as our model photoelastic material. Within the range of possible photoelastic

Table 1
Material properties of Homalite-100

Property	Homalite-100	
	Static (strain rate $\sim 10^{-3}$/s)	Dynamic (strain rate $\sim 10^3$/s)
Density ρ(kg/m^3)	1230	1230
Young's modulus (GPa)	3.45	
Dilatational wave speed c_l (m/s) (plane stress)	1890	2119
Shear wave speed c_S (m/s)	1080	1208
Rayleigh wave speed c_R (m/s)	1010	1110
Poisson's ratio v	0.35	0.35
Material fringe constant f_σ (kN/m)	23.7	
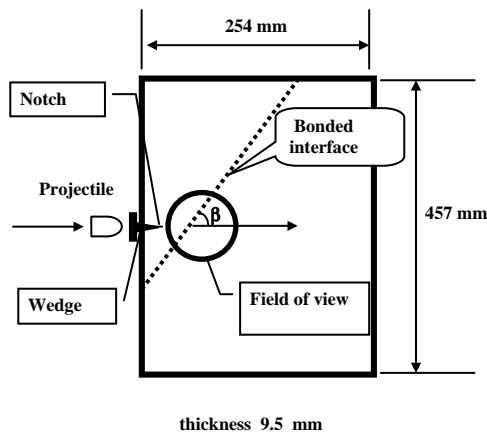
Fig. 3. The wedge-loaded pre-notched specimen geometry.

materials, Homalite-100 was chosen because its dynamic fracture behavior has been documented widely in literature. Indeed the variation of dynamic fracture toughness of monolithic Homalite with crack speed has been studied in the early years of the dynamic fracture discipline (Dally, 1979; Fourney et al., 1983; Kalthoff, 1983). These results are used in relation to the analytical model described in Section 4. Some of the physical properties of Homalite-100 are listed in Table 1. The quasi-static values were obtained from the literature while the dynamic values were measured by the authors (Xu and Rosakis, 2002a).

A novel wedge-loaded plate specimen was designed to produce a single, straight dynamic crack propagating towards the weakly bonded, inclined interface as shown in Fig. 3. The wedge is inserted into a pre-notch and when it is impacted by a projectile,

Table 2
Interfacial strengths and mode-I fracture toughnesses of different bonds

Interface	Tensile strength σ_c(MPa)	Shear strength τ_c(MPa)	Fracture toughness	
			K_{IC} (MPa m$^{1/2}$)	Γ_{IC} (J/m^2)
Homalite//Weldon-10// Homalite (strong)	7.74	> 21.65	0.83	199.7
Homalite//polyester// Homalite		> 23.26	0.56	90.9
Homalite//384//Homalite (weak)	6.75	7.47	0.38	41.9

the wedge opens the notch faces producing a single mode-I crack which is driven towards the inclined interface. The initial crack tip speed is related to the impact speed of the projectile. The advantage of this type of dynamic loading is the generation of a negative T-stress which enhances crack path stability and retards branching as the crack tip speed reaches certain levels (Cotterell and Rice, 1980). Wedge-loaded specimens of various types have been used extensively in previous static and dynamic fracture experiments (Hahn et al., 1980; Thouless, 1992; Guduru et al., 2001).

The specimen's sizes were large enough such that the major stress waves reflecting from free boundaries entered the field of view, 20 µs after the incident crack reached the interface. After numerous preliminary tests, the in-plane specimen size was fixed to be 457 mm long, 254 mm wide and the plate thickness was 9.5 mm. Inclined interfaces were cut and covered several characteristic interfacial angles. These angles were $10°, 30°, 45°, 60°$ and $90°$. To provide different interfacial strengths and fracture toughnesses, two kinds of adhesives, Weldon-10 and Loctite 384, were used to bond the interfaces and to create weak interfaces of toughness less than that of monolithic Homalite. The interfacial bond strengths and the fracture toughnesses were measured by the authors and are listed in Table 2 (Xu et al., 2002). The Weldon-10 adhesive is considered to be a "strong" adhesive. The Loctite 384 formed a "weak" bond. The average thickness of all adhesive layers was less than 20 µm.

2.2. Experimental setup

A schematic of the dynamic photoelasticity setup used in this study is given in Fig. 4. Two sheets of circular polarizer were placed on either side of the specimen. The coherent, monochromatic, plane polarized laser output is collimated to a beam of 100 mm in diameter. The laser beam is transmitted through the specimen. The resulting fringe pattern is recorded by the high-speed camera. A Cordin model 330A rotating mirror type high-speed film camera is used to record the images. During the impact test, a projectile was fired by the gas gun and impacted the loading wedge to trigger the recording system and to dynamically initiate the mode-I incident crack. Details of experiments were reported by Xu and Rosakis (2002a). Under the dynamic deformation, the generation of isochromatic fringe patterns is governed by the stress optic law.
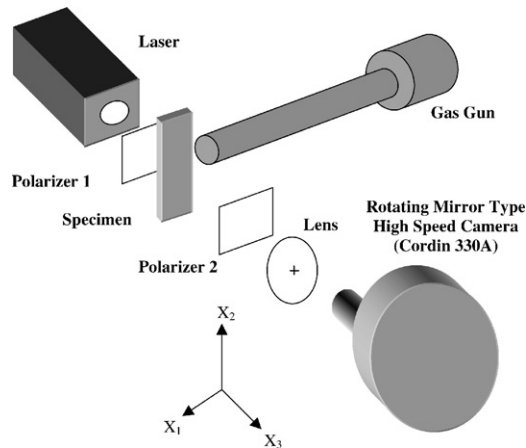
Fig. 4. Schematic of the dynamic photoelasticity setup.

For the case of monochromatic light, the isochromatic fringe patterns observed are proportional to contours of constant maximum in-plane shear stress, $\hat{\tau}_{max} = (\hat{\sigma}_1 - \hat{\sigma}_2)/2$.

3. Experimental observations

In order to systematically study the effects of interfacial angles, bond strengths and impact speeds on the dynamic crack penetration/deflection behavior at interfaces, a baseline impact speed of 19–20 m/s was chosen in order to produce a single mode-I crack without inducing crack branching at the pre-notch. Then, for the same interfacial bonding strength, different interfacial angles were tested.

3.1. Crack deflection/penetration at a weak interface

Fig. 5 shows a series of dynamic photoelasticity images of the crack deflection process at a weak interface whose interfacial angle is 10°. The impact speed was 27 m/s. The vertical line appearing in every image is the camera streak line, which is used for positioning and reference purposes. Another almost horizontal thin line reveals the position of the interface. The dark circular spot, at the center and just above the interface, is a scaling mark of 6.35 mm in diameter. In Fig. 5(b), a mode-I crack is seen propagating towards the inclined interface at a high speed. The incident mode-I crack reached the interface at around 110 μs after the impact. Then it transits into a mixed-mode interfacial crack as shown in Figs. 5(c) and (d). The small asymmetry in the fringe patterns of the interfacial crack reveals the existence of a small mode mixity. The crack length vs. time record is shown in Fig. 5(e). The noticeable change of slopes at around 120 μs indicates a significant increase of the cracks tip speed after the crack deflection. The average speed of the incoming crack is approximately 407 m/s. After crack deflection at the interface, the average interfacial crack speed is around 988 m/s.
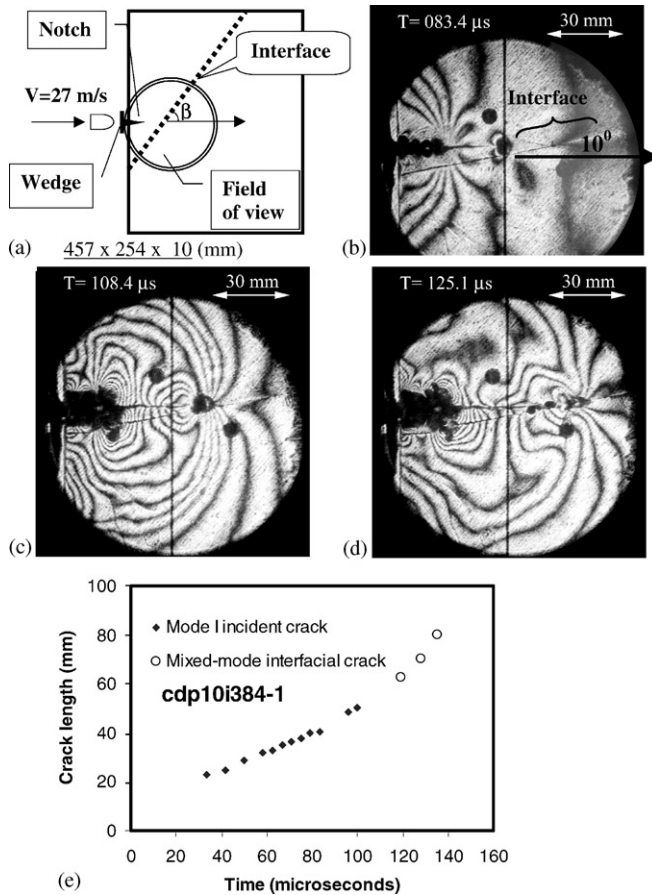
Fig. 5. Crack deflection process at a weak interface (interfacial angle $10°$) and crack length history before and after crack deflection at a weak interface (interfacial angle $10°$).

In the experiment described above, an impact speed of 27 m/s was employed and strong fringe patterns during the crack deflection process were observed. In the next experiment, a relatively lower impact of 19–20 m/s was intentionally chosen to reduce the spurious stress waves caused by projectile impact. Fig. 6 shows the crack deflection process at a weak interface whose interfacial angle is $30°$. In Fig. 6(b), a dynamically propagating mode-I crack (surrounded by symmetric fringe patterns) is seen to propagate towards the interface. Around 164 μs after impact, we notice that the crack tip fringe pattern has already started to lose some of its symmetry. Around 170 μs (Fig. 6(d)), this mode-I incident crack has already transited into a mixed-mode crack at the interface whose fringe pattern at the crack tip was clearly asymmetric with respect to its propagation direction. In fact, a close look at this pattern reveals that its line of symmetry is still parallel to the horizontal line although the crack propagates along
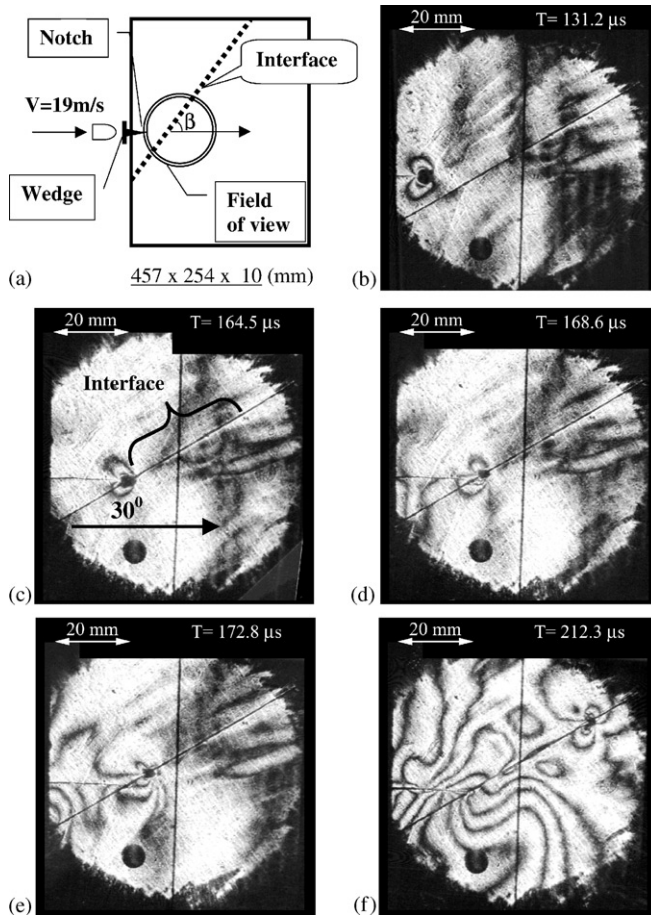
Fig. 6. Crack deflection process at a weak interface (interfacial angle 30°).

the inclined weak interface. Also, the caustic (or shadow spot surrounding the crack tip) size at the crack tip was significantly reduced in comparison to the caustic sizes in Figs. 6(b) and (c). As the interfacial crack quickly moved out of the field of view, the horizontal crack faces of the original mode-I crack are seen to experience clear frictional contact as evident from the Fig. 6(f).

The abruptness of the transition behavior between a mode-I incident crack and a mixed-mode interfacial crack can be graphically witnessed by the impressive jump in crack speed across the interface. Fig. 7(a) shows the total crack length history as the incident mode-I crack develops and transitions into a mixed-mode interfacial crack. The interfacial crack length used in Fig. 7(a) is defined as the total instantaneous arc length measured along the non-uniform crack path. Differentiation of the crack length record furnishes the tangential crack tip speed before and after crack deflection. Since the differentiation process is based on a three-point fitting of the crack length history, the
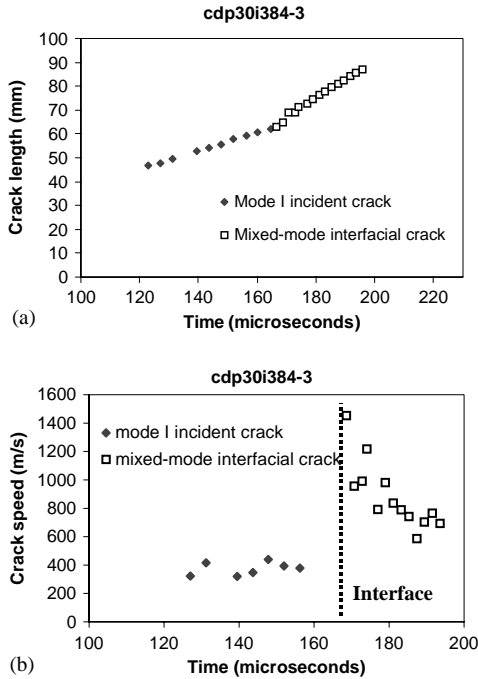
Fig. 7. Crack length history (a) and crack speed history (b) before and after crack deflection at a weak interface (interfacial angle 30°).

exact crack speed at the interface could not be obtained. Before deflection, the crack tip speed is approximately 400 m/s, which is a speed very close to the branching speed of Homalite-100. After crack deflection, the speed jumped by as much as 800–1000 m/s and then decreased as it propagated further along the interface.

The next two experiments were conducted for different interfacial angles of 45° and 60°, respectively. The incident crack reached the interface around 153 μs after impact as seen in Fig. 8(a). It is observed that the symmetric fringe pattern of the incident mode-I crack disappeared as soon as the crack deflected into the interface. The shape of the fringe pattern of Fig. 8(b) suggests that this interfacial crack is shear dominated at the latter propagation stage. In Fig. 8(c), it is interesting to observe that after this shear-dominated crack propagated some distance along the interface, some secondary cracks were formed at one side of the interface. These secondary cracks are locally mode-I and form on the tension side of the sheared interface. They form after the dominant crack has propagated along the interface and thus after the interface has already failed in shear. These types of secondary cracks that are a by-product of shear crack growth along interfaces have already been observed experimentally (Rosakis and Ravichandran, 2000; Xu and Rosakis, 2002a) and are always associated with dynamic shear-dominated crack growth along weak interfaces. As the interfacial angle is changed to 60°, the dynamic crack deflection behavior is slightly altered. As shown in Fig. 8(d),
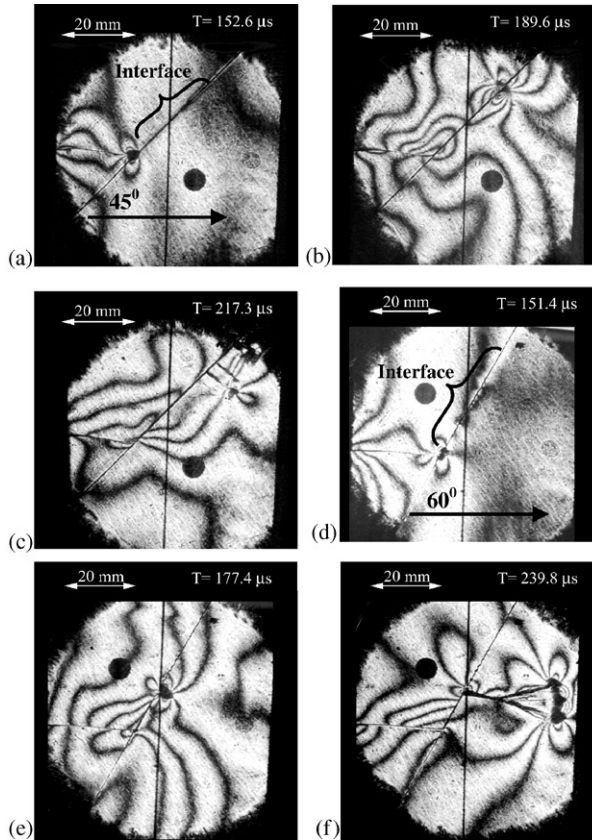
Fig. 8. Comparison of crack deflection process at a weak interface: (a)–(c) interfacial angle 45° and (d)–(f) interfacial angle 60°.

the incident mode-I crack approached the interface at about 151 μs after impact and transitioned into a mixed-mode interfacial crack. At around 177 μs, this mixed-mode interfacial crack kinked into the right side of the interface. A significant caustic (or shadow spot) as shown in Fig. 8(e) shows the mode-I nature of the kinked crack. The speed of the kinked crack, which moved into the homogeneous Homalite part, was high enough to induce multiple branches which are visible in Fig. 8(f). The whole process is reflected in the crack speed and length records, which are shown in Fig. 9. First, we notice the crack speed jump across the interface at about 150 μs. Obviously, the initial interfacial crack speed of 700 m/s is much higher than the incident crack speed, which is about 400 m/s for the interfacial angle 60° case. However, the interfacial crack speed reduced to 350 m/s soon after the interfacial crack kinked into the right side of monolithic Homalite. The experiment also suggests that just before the crack kinking, there was a brief crack speed reduction characteristically seen in several failure mode transition experiments (Xu and Rosakis, 2002b). In Fig. 9, the comparison of the crack
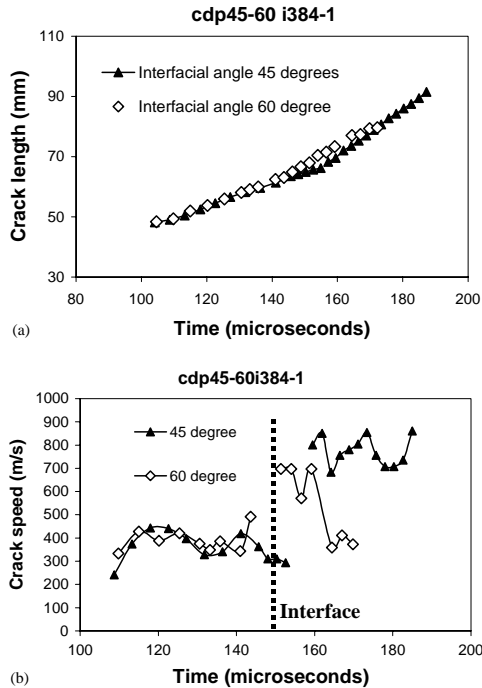
Fig. 9. Crack length history (a) and crack speed history (b) before and after crack deflection at a weak interface.

length and speed history is made for two different interfacial angle cases. It is noticed that the interfacial crack speed for the interfacial angle 45° case is always higher than that for the interfacial angle 60° case. This experimental phenomenon will be analyzed by the proposed dynamic fracture mechanics model.

The above results clearly elucidate the role of interface inclination in the nature of failure mode transition. In the following section, we will concentrate on the role of the interfacial strength in the same phenomenon. We also expect that interfacial bond strengths are essential to the determination of the dynamic crack deflection/penetration behavior (Needleman and Rosakis, 1999; Xu and Rosakis, 2002c).

3.2. Crack deflection/penetration at a strong interface

In the set of experiments described in this section, we examine interfaces inclined at exactly the same angles as in Section 3.1 and incident mode-I cracks propagating with speeds that are nominally the same as before. The only difference is in the interfacial bond strength, which is higher than in the previous case. Fig. 10 shows a series of photoelasticity snap shots following impact of two specimens featuring the strong interfacial bond and interfacial angles of 10° and 30°, respectively. Around 133 μs after impact, the mode-I incident crack has just reached the interface as shown in Fig. 10(a).
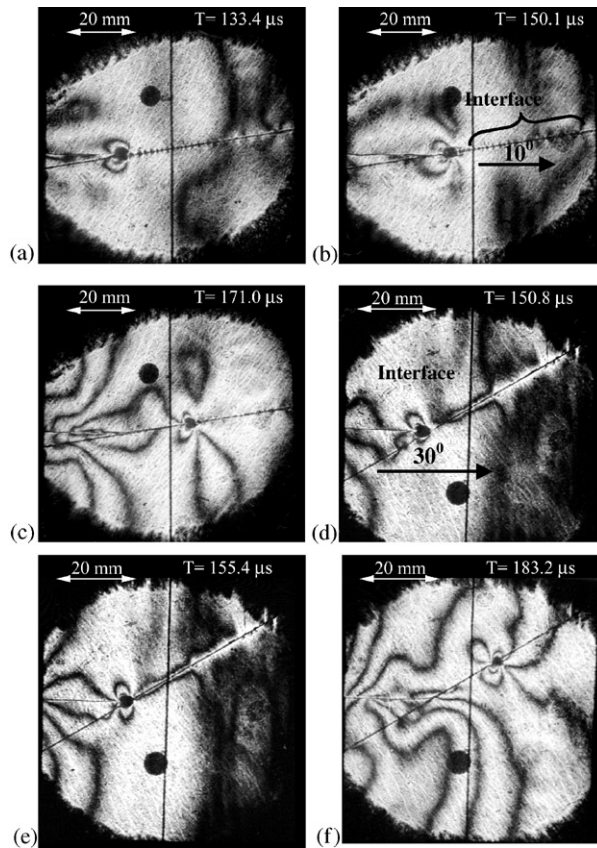
Fig. 10. Comparison of crack deflection processes at strong interfaces: (a)–(c) interfacial angle 10°. (d)–(f) interfacial angles 30°.

We notice that, at this moment, the crack tip fringes still had a symmetric pattern. At 150 μs, this mode-I crack transitioned into a mixed-mode crack at the interface in a manner very similar to the case described in the previous section (see Fig. 6(d)). Figs. 10(d)–(f) show the dynamic crack deflection at a strong interface whose interfacial angle is 30°. Around 150 μs after impact, the incident crack approached the interface. Later on, it induced a deflected interfacial crack which propagated along the interface only. The crack speed record is shown in Fig. 11 and it is qualitatively similar to the previous cases, i.e., a significant crack speed jump after crack deflection.

The last case considered in this section (see Fig. 12) is the one involving an interfacial angle of 60°. In this case, the interfacial crack kinked only slightly off its original path and then accelerated again into the right side of the interface reaching branching conditions at 235 μs after impact (see Fig. 12(f)). The experiment suggests that for this "strong" interface, the interfacial angle of 60° is very close to the critical angle above which a crack penetration of this interface is possible. Fig. 12 should be compared
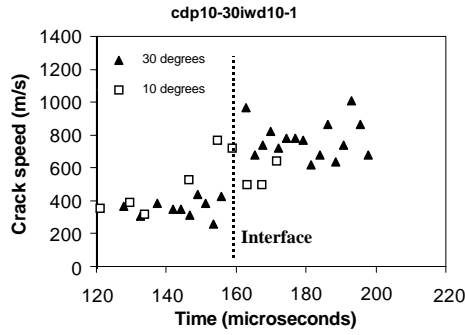
Fig. 11. Comparison of crack speed history before and after crack deflection at a strong interface for interfacial angle 10° and 30°.
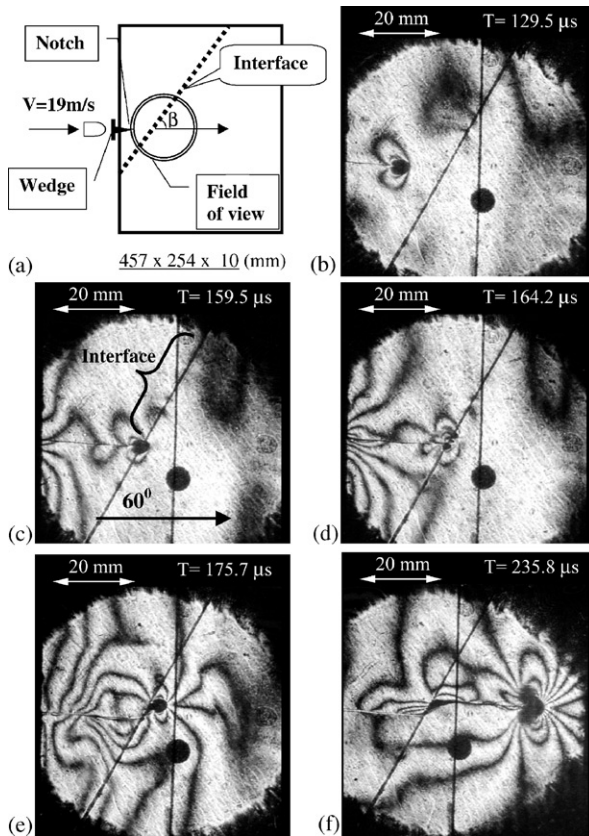
Fig. 12. Crack deflection and subsequent penetration at a strong interface (interfacial angle 60°).

to Fig. 8(d)–(f) where a weaker interface (also at $60°$) was tested under nominally the same conditions. The differences between the deflection/penetration behavior of Fig. 8(f) and 12(f) are evident.

4. A model for dynamic crack deflection/penetration

Fig. 13 shows a schematic diagram describing the geometry relevant to the dynamic crack deflection/kinking problem. Two identical homogeneous and isotropic elastic solids are bonded along an interface indicated here by the dashed line. The Young's and shear moduli, Poisson's ratio and mass density are denoted by E, μ, υ and ρ, respectively. Before reaching the interface, a dynamic mode-I crack propagates within the homogeneous solid towards the inclined interface (Fig. 13(a)). The angle between the crack plane and the interface is denoted by β. The critical question to be addressed is whether this mode-I crack will continue to propagate on the original crack plane ($x_2 = 0$) after encountering the interface (Fig. 13(a)), or it will kink out to propagate along the interface and become a mixed-mode interfacial crack (Fig. 13(b)). It is anticipated that the former (continuous crack propagation along the original crack plane) and the latter (crack deflection) modes occur for strong and weak interfaces, respectively.
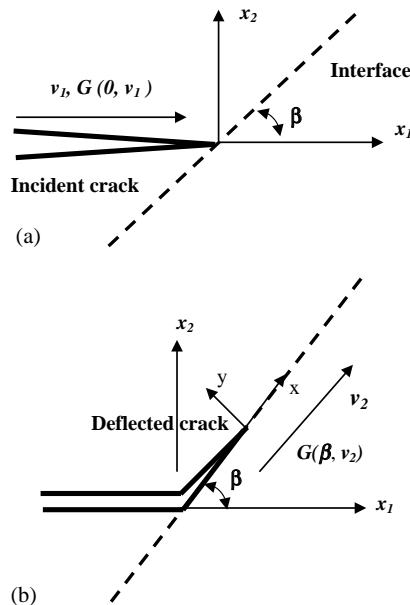
Fig. 13. Schematic diagram showing a mode-I crack arriving (a) and subsequently deflecting at a weak interface between two identical homogeneous solids (b).

4.1. Static crack kinking/deflection analysis

He and Hutchinson (1989) studied the competition between the two fracture modes of continuous crack propagation on the crack plane and crack kinking along a bimaterial interface subjected to remote static loading. An extensive discussion of this phenomenon was described by Hutchinson and Suo (1992). Once the two constituents have identical elastic properties (as in the present constitutively homogeneous material system), the analysis becomes very simple, as described in the following.

For a mode-I crack subjected to a remote static stress intensity factor, $K_{\mathrm{I}}^{\mathrm{s}}$, continuous crack propagation within the crack plane occurs when the mode-I static crack energy release rate, $G_{\mathrm{I}}^{\mathrm{s}}$, reaches the fracture toughness $\Gamma_{\mathrm{IC}}^{\mathrm{MA}}$ of the matrix material, i.e.,

$$G_{\mathrm{I}}^{\mathrm{s}} = \frac{1 - v^2}{E}(K_{\mathrm{I}}^{\mathrm{s}})^2 = \Gamma_{\mathrm{IC}}^{\mathrm{MA}}. \tag{1}$$

On the other hand, the crack will deflect/kink at the interface when the static energy release rate of the kinked/deflected crack tip, G^{sk}, reaches or exceeds the fracture toughness of the interface, $\Gamma_{\mathrm{c}}^{\mathrm{IT}}$, i.e.,

$$G^{\mathrm{sk}} = \frac{1 - v^2}{E}[(K_{\mathrm{I}}^{\mathrm{sk}})^2 + (K_{\mathrm{II}}^{\mathrm{sk}})^2] = \Gamma_{\mathrm{c}}^{\mathrm{IT}}, \tag{2}$$

where $K_{\mathrm{I}}^{\mathrm{sk}}, K_{\mathrm{II}}^{\mathrm{sk}}$ are static mode-I and mode-II stress intensity factors for the deflected (kinked) mixed-mode crack, and they are related to the remote mode-I stress intensity factors before crack deflection at the interfaces as a function of the kinking angle β (interfacial angle) (Hutchinson and Suo, 1992; Anderson, 1995):

$$K_{\mathrm{I}}^{\mathrm{sk}} = K_{\mathrm{I}}^{\mathrm{s}} \left(\frac{3}{4} \cos \frac{\beta}{2} + \frac{1}{4} \cos \frac{3\beta}{2} \right),$$

$$K_{\mathrm{II}}^{\mathrm{sk}} = K_{\mathrm{I}}^{\mathrm{s}} \left(\frac{1}{4} \sin \frac{\beta}{2} + \frac{1}{4} \sin \frac{3\beta}{2} \right). \tag{3}$$

From the ratio of Eqs. (2) and (1), the critical conditions governing these two fracture modes are as follows:

$$\frac{G^{\mathrm{sk}}}{G_{\mathrm{I}}^{\mathrm{s}}} < \frac{\Gamma_{\mathrm{c}}^{\mathrm{IT}}}{\Gamma_{\mathrm{Ic}}^{\mathrm{MA}}} \tag{4a}$$

for the continuous crack propagation (crack penetration) along the original crack plane and

$$\frac{G^{\mathrm{sk}}}{G_{I}^{\mathrm{s}}} \geqslant \frac{\Gamma_{\mathrm{c}}^{\mathrm{IT}}}{\Gamma_{\mathrm{Ic}}^{\mathrm{MA}}} \tag{4b}$$

for the crack deflection/kinking at the interface. It is observed from Eqs. (1)–(3) that the ratio of two energy release rates depends only on the kinking (interfacial) angle and not on the value of the stress intensity factor or material properties:

$$\frac{G^{\mathrm{sk}}}{G_{\mathrm{I}}^{\mathrm{s}}} = \frac{1}{16} \left[\left(3 \cos \frac{\beta}{2} + \cos \frac{3\beta}{2} \right)^2 + \left(\sin \frac{\beta}{2} + \sin \frac{3\beta}{2} \right)^2 \right]. \tag{5}$$

It is pointed out that the above expression for the energy release rate ratio holds for both plane strain and plane stress analyses.

4.2. Dynamic crack propagation in the crack plane

Let v_1 denote the crack tip speed prior to reaching the interface. The dynamic energy release rate around the mode-I, plane strain crack tip is given by (e.g., Freund, 1990; Broberg, 1999)

$$G_{\mathrm{I}}^{\mathrm{d}} = \frac{1 - v^2}{E} [A_{\mathrm{I}}(v_1)(K_{\mathrm{I}}^{\mathrm{d}}(v_1))^2], \tag{6}$$

where $K_{\mathrm{I}}^{\mathrm{d}}$ is the dynamic stress intensity factor of the incident mode-I crack. A_{I} is a universal function of crack tip speed v_1, given by

$$A_{\mathrm{I}}(v) = \frac{v^2 \alpha_{\mathrm{d}}}{(1 - v)c_{\mathrm{S}}^2 D}, \tag{7}$$

where

$$
\begin{aligned}
&D = 4\alpha_{\mathrm{s}}\alpha_{\mathrm{d}} - \left(1 + \alpha_{\mathrm{s}}^2\right)^2 \\
&\alpha_{\mathrm{s}} = \sqrt{1 - (v/c_{\mathrm{S}})^2}, \quad \alpha_{\mathrm{d}} = \sqrt{1 - (v/c_{\mathrm{d}})^2} \\
&c_{\mathrm{S}} = \sqrt{\frac{\mu}{\rho}}, \quad c_{\mathrm{d}} = \sqrt{\frac{\kappa + 1}{\kappa - 1}}c_{\mathrm{S}} \\
&\kappa = \begin{cases} 3 - 4v \ \ (\text{plane strain}) \\ \dfrac{3 - v}{1 + v} \ \ (\text{plane stress}) \end{cases}
\end{aligned}
\tag{8}
$$

and c_{S} and c_{d} are the shear wave and dilatational wave speeds of the matrix material. Under certain circumstances, the dynamic crack stress intensity factor $K_{\mathrm{I}}^{\mathrm{d}}$ can be related to its static counterpart $K_{\mathrm{I}}^{\mathrm{s}}$ through a "universal function of crack tip speed", $k_{\mathrm{I}}(v)$ (Freund, 1990):

$$K_{\mathrm{I}}^{\mathrm{d}} = k_{\mathrm{I}}(v_1)K_{\mathrm{I}}^{\mathrm{s}}, \tag{9}$$

where the universal function of crack tip speed depends on the material properties through the elastic wave speeds, but it is independent of the loading on the body:

$$k_{\mathrm{I}}(v) = \frac{1 - v/c_R}{S_{\mathrm{t}}(1/v)\sqrt{1 - v/c_{\mathrm{d}}}}, \tag{10}$$

where c_R is the Rayleigh wave speed of the material. For most practical purposes, $S_{\mathrm{t}}(1/v) \approx 1$. The crack will continue to propagate in the crack plane if the dynamic energy release rate of the mode-I incident crack reaches the corresponding dynamic fracture toughness $\Gamma_{\mathrm{Id}}^{\mathrm{MA}}(v_1)$ of the matrix materials, i.e.,

$$G_{\mathrm{I}}^{\mathrm{d}} = \frac{1 - v^2}{E} A_{\mathrm{I}}(v_1)[k_{\mathrm{I}}(v_1)K_{\mathrm{I}}^{\mathrm{s}}]^2 = \Gamma_{\mathrm{Id}}^{\mathrm{MA}}(v_1), \tag{11}$$

where Eqs. (6) and (9) have been used.

4.3. Dynamic crack deflection/kinking along the interface

As shown in Fig. 13(b), let v_2 denote the speed of the deflected crack tip at the instant right after deflection, and let K_I^{dk} and K_{II}^{dk} be the dynamic mode-I and mode-II stress intensity factors for the deflected (kinked) mixed-mode crack. We will assume that the universal relation Eq. (9) between the dynamic and static stress intensity factors also holds for the deflected crack tip, i.e.,

$$K_I^{dk} = k_I(v_2)K_I^{sk},$$
$$K_{II}^{dk} = k_{II}(v_2)K_{II}^{sk}, \tag{12}$$

where the static stress intensity factors around the deflected crack tip are given in Eq. (3). In the above equation, k_I is the same universal function in Eq. (10) for mode-I dynamic crack propagation (though it is a function of the speed of the deflected crack), k_{II} is the universal function for mode-II dynamic crack propagation and is the same as k_I in Eq. (10) except that the dilatational wave speed c_d is replaced by the shear wave speed c_S (Freund, 1990), i.e.,

$$k_{II}(v) \cong \frac{1 - v/c_R}{\sqrt{1 - v/c_S}}. \tag{13}$$

The dynamic energy release rate around the deflected crack tip is then related to the corresponding dynamic crack tip stress intensity factors by

$$G^d = \frac{1 - v^2}{E}[A_I(v_2)[K_I^{dk}]^2 + A_{II}(v_2)[K_{II}^{dk}]^2], \tag{14}$$

where A_{II} is given by (e.g., Freund, 1990)

$$A_{II}(v) = \frac{v^2 \alpha_s}{(1 - v)c_S^2 D(v)}. \tag{15}$$

The crack will deflect at the interface if the dynamic energy release rate around the deflected crack tip reaches or exceeds the corresponding fracture toughness of the interface, i.e.,

$$G^d = \frac{1 - v^2}{E}[A_I(v_2)[k_I(v_2)K_I^{sk}]^2 + A_{II}(v_2)[k_{II}(v_2)K_{II}^{sk}]^2] \geqslant \Gamma_c^{IT}(v_2). \tag{16}$$

4.4. Critical condition for dynamic crack deflection at the interface

Similar to the static case, we may use the ratio of dynamic crack energy release rates in Eqs. (11) and (16) to determine the critical condition for dynamic crack deflection at the interface. The advantage of using the ratio of Eqs. (11)–(16) is that the remote stress intensity does not come into play and as a result the resulting criterion for dynamic crack deflection depends only on the interfacial angle β, the crack tip speeds v_1 and v_2, and the shear and longitudinal wave speeds c_S and c_d. Using Eqs. (7) and (1) for A_I and A_{II}, respectively, and the relation (3) between the static stress intensity

(a)

(b)
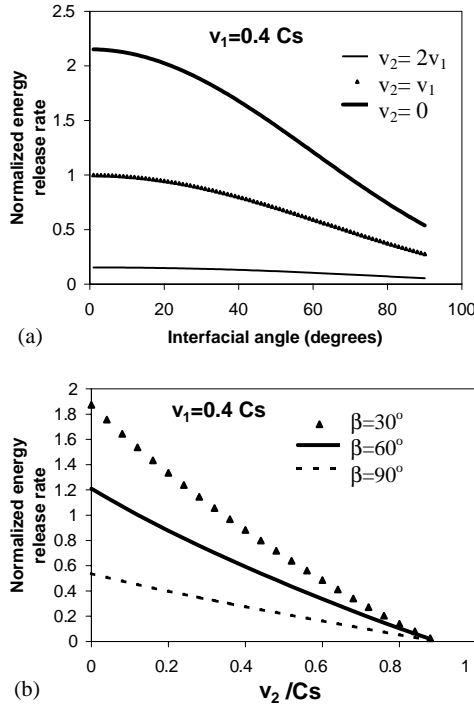
Fig. 14. The energy release rate (driving force) for a deflected crack of speed v_2 normalized with the energy release rate of the incident mode-I crack (speed $v_1 = 0.4c_S$) as a function of v_2 and interfacial angle.

factors, we have determined the ratio of two energy release rates for the deflected (kinked) interfacial crack and the incident mode-I crack:

$$\frac{G^d(\beta, v_2)}{G_I^d(v_1)} = \frac{A_I(v_2)k_I^2(v_2)(3\cos\frac{\beta}{2} + \cos\frac{3\beta}{2})^2 + A_{II}(v_2)k_{II}^2(v_2)(\sin\frac{\beta}{2} + \sin\frac{3\beta}{2})^2}{16A_I(v_1)k_I^2(v_1)}$$

$$= \left(\frac{v_2}{v_1}\right)^2 \frac{D_1}{D_2} \frac{\alpha_{d2}k_I^2(v_2)(3\cos\frac{\beta}{2} + \cos\frac{3\beta}{2})^2 + \alpha_{s2}k_{II}^2(v_2)(\sin\frac{\beta}{2} + \sin\frac{3\beta}{2})^2}{16\alpha_{d1}k_I^2(v_1)}.$$

(17)

It should be pointed out that, similar to its counterpart (5) for the static case, the above ratio holds for both plane strain and plane stress analyses. From Eqs. (16) and (11), the crack deflection criterion can be stated as follows:

$$\frac{G^d(\beta, v_2)}{G_I^d(v_1)} \geqslant \frac{\Gamma_c^{IT}(v_2)}{\Gamma_{Id}^{MA}(v_1)}.$$

(18)

It should be noted at this point that, for fixed β and v_1, the ratio in the left side of Eq. (18) vanishes for $v_2 = c_R$ and is maximized for $v_2 = 0$. This is evident from Fig. 14 where this ratio is plotted as a function of v_2 for various interfacial angles β.

Simple inspection of Eq. (17) shows that this behavior is a consequence of the speed dependence of universal functions $k_I(v)$ and $k_{II}(v)$ which vanish at $v = c_R$. The behavior of this ratio necessitates that the above deflection criterion is reduced to

$$\underset{v_2}{\text{Max}} \left\{ \frac{G^d(\beta, v_2)}{G_I^d(v_1)} \right\} = \frac{G^d(\beta, 0)}{G_I^d(v_1)} \geqslant \frac{\Gamma_c^{IT}(v_2)}{\Gamma_{Id}^{MA}(v_1)}. \tag{19}$$

If the criterion is indeed satisfied and the crack deflects into the interface, its speed v_2 will be such that relation (18) holds as a pure equality. Then,

$$\frac{G^d(\beta, v_2)}{G_I^d(v_1)} = \frac{\Gamma_c^{IT}(v_2)}{\Gamma_{Id}^{MA}(v_1)} \tag{20}$$

and the above equation will provide an expression for v_2, as a function of the incident crack tip speed v_1, and the ratio of interfacial to matrix toughnesses (right-hand side of Eq. (20)). The toughness ratio will itself, in general, be a function of the crack tip speeds v_1 and v_2. Indeed, $\Gamma_{Id}^{MA}(v_1)$ is the dynamic fracture toughness of the matrix material (Homalite-100 in this experiment), which is a function of crack speeds that has been measured in experiments by Kobayashi and Mall (1978) and Dally (1979). In nominally brittle homogeneous materials such as Homalite-100, PMMA and glass, the functional form $\Gamma_{Id}^{MA}(v_1)$ is typically monotonically increasing from a quasi-static crack growth value to much larger levels achieved just before the branching speed is reached (Rosakis and Ravichandran, 2000). Indeed, as a crack increases its speed, it starts generating local microkinks, or abortive branches, whose number drastically multiplies just before final branching occurs. By doing so, the total energy spent in crack growth (toughness) increases drastically (Ravi-Chandar and Knauss, 1984; Sharon and Fineberg, 1999), accounting for the observed drastic increase of toughness with speeds close to 0.3–0.4c_S. In the presence of weak paths, bonds or interfaces, the situation is often very different. The weak path suppresses any off-plane microbranches that might develop as a mode-I crack accelerates along its length (Lee and Knauss, 1989; Washabaugh and Knauss, 1994). This effect deactivates the mechanism of fracture toughness increase with speeds, described above for purely homogeneous monolithic solids, and allows a crack to reach speeds as high as the Rayleigh wave speed of the surrounding bulk solids without any increase in fracture toughness (Washabaugh and Knauss, 1994; Coker and Rosakis, 2002). Weak fracture paths and bonds can also trap mixed-mode or mode-II propagating cracks. Indeed depending on the detailed bond characteristics, mixed-mode cracks can often become very fast and may (unlike their mode-I equivalent) become intersonic as shown in a series of recent studies (Lambros and Rosakis, 1995; Rosakis et al., 1999; Coker and Rosakis, 2002). Consistent with the above discussion, we will assume in this work that the interfacial fracture toughness is independent of the crack speed and of the mode mixity. We believe this second assumption to be a good assumption for most mixity levels especially because the materials to the right and left of the bonds are identical (Hutchinson and Suo, 1992). Following these assumptions, Eq. (20) which determines the interfacial crack tip speed v_2 as a function of the speed v_1 of the incident mode-I crack is

$$\frac{G^d(\beta, v_2)}{G_I^d(v_1)} = \frac{\Gamma_c^{IT}}{\Gamma_{Id}^{MA}(v_1)}. \tag{21}$$

5. Results and discussions

5.1. Deflection vs. penetration

To determine whether an incident crack will penetrate an interface, the normalized energy release rate, which is the left-hand side of Eq. (19), is plotted as a function of angle β, at the particular speed of incidence v_1. Examples of such plots are seen in Figs. 15 and 16. The right-hand side of this equation is then estimated from experimental measurements of the fracture toughness of the bond and the bulk Homalite at crack growth speed v_1. The data for the variation of dynamic fracture toughness with speeds were reported by Fourney et al. (1983), Kalthoff (1983), Kobayashi and Mall (1978).

We first start by applying this methodology to the experiments briefly discussed in Fig. 2 (Xu and Rosakis, 2002a). In this case, the bond involved in a polyester adhesive and its fracture toughness is 0.56 MPa$\sqrt{m}$ (Xu and Rosakis, 2002a). The incident crack speed was about 300 m/s. The fracture toughness of Homalite at this crack speed is about 0.6 MPa$\sqrt{m}$ (Kobayashi and Mall, 1978), making the ratio $\Gamma_c^{IT}/\Gamma_{Id}^{MA}$ on the right-hand side of Eq. (19) equal to 0.93. Fig. 15 displays a graphic representation of the inequality (19). Indeed, according to the criterion, deflection into the interface will take place at $0 < \beta < 59°$ while the interface will be penetrated for $59° < \beta < 90°$. It should be noted that both cases displayed in Fig. 2 are consistent with this prediction.

For the inclined interface experiments presented here in Section 3, the incident crack speed varied between 350 and 450 m/s ($0.252–0.377c_S$) and the corresponding dynamic fracture toughness of Homalite-100 varied from 0.75 to 1.4 MPa, respectively. Recognizing a certain level of uncertainty in the experimental measurement of crack tip speeds and toughness (both bond and Homalite), average values of these parameters were taken. Fig. 16(a) and (b) describe the predicted crack deflection/penetration regimes for the two types of bonds described in Table 2 and are used in the experiments presented in Section 3. It should be noted here that for the case of a weak bond (Loctite-384 adhesive), there is no intersection of the horizontal line (toughness ratio)
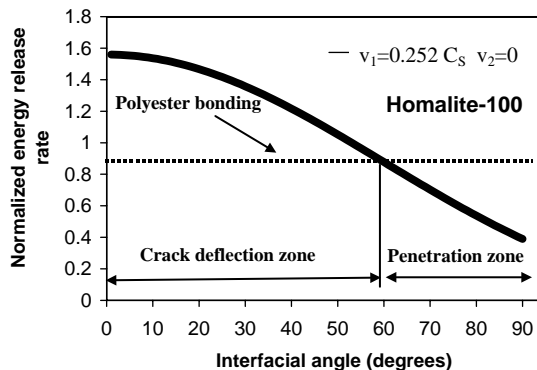
Fig. 15. Prediction of the dynamic crack deflection/penetration regimes for a crack traveling at 300 m/s towards an interface bonded by a polyester adhesive.
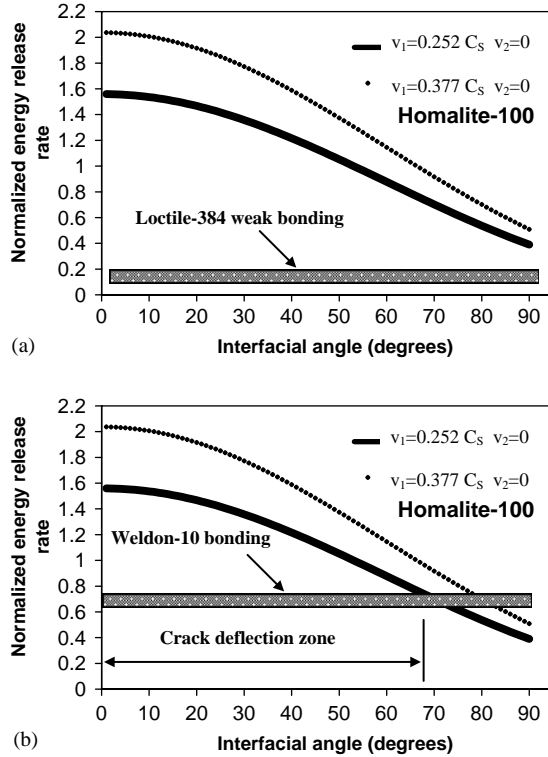
Fig. 16. Prediction of the dynamic crack deflection and penetration regimes at interfaces for a weak bond (a) and for a strong bond (b).

with the left-hand side of Eq. (19) at speeds v_1 such that $0.252 < v_1 < 0.377c_S$. This means that the crack will always deflect into the interface as is the case in Figs. 5, 6, and 8. For a higher bond strength case (Weldon-10 adhesive), the crack will deflect into the interface for all $\beta < 68°$ and will penetrate the interface for all $68° < \beta < 90°$. This is consistent with the result of Figs. 10, and 12. Indeed, for interface angles 10° and 30°, the crack is clearly deflected. On the other hand, for interfacial angle of 60° (see Fig. 12), the crack kinked slightly but very soon penetrated the interface suffering only a small temporary deflection. This is consistent with the fact that, within experimental error, 60° is very close to the end of crack deflection zone. It should be noted at this point that the horizontal levels of toughness ratio are represented in Fig. 16 as bands to reflect maximum uncertainties in incident crack tip speeds v_1.

5.2. Predictions of the interfacial crack speeds

For a certain speed of the incident mode-I crack and if the interfacial angle and the bond strength are such that the criterion of Eq. (19) predicts crack deflection at the interface, then the interfacial crack speed can be predicted by Eq. (20). This

(a)

(b)
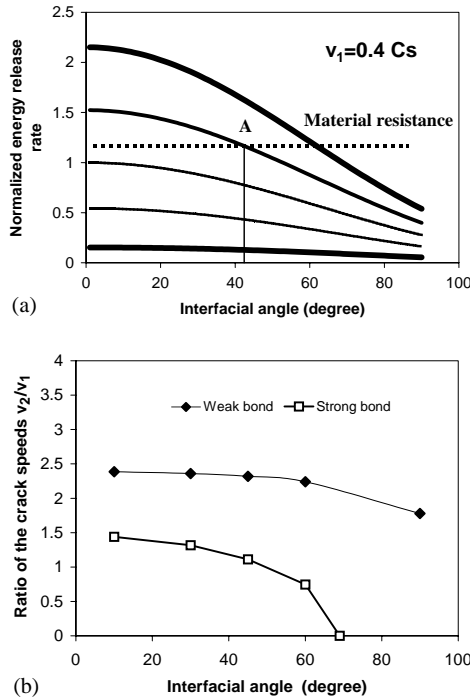
Fig. 17. Methodology for predicting interfacial crack speed following deflection (a) and effect of the interfacial fracture toughness on deflected interfacial crack speeds for the case of incident crack speed of 400 m/s (b).

Table 3
Comparison of predicted and measured interfacial crack speeds

Angles($^\circ$)	Strong interface		Weak interface	
	Predicted (m/s)	Experimental (m/s)	Predicted (m/s)	Experimental (m/s)
10	576	534		
30	559	766	944	1100/920
45			928	800
60			896	700

procedure is graphically illustrated in Fig. 17(a). This figure shows the variation of the normalized energy release as a function of interfacial angle for a fixed incident crack speed $v_1 = 0.4c_S$. This ratio depends on v_2 parametrically. The figure also displays the normalized material resistance level for this specific v_1 as a dotted line. For the specific interfacial angle under consideration, a vertical line is drawn to intersect the dotted line at a point A. The speed $v_2 = kv_1$ is then adjusted in such a way as to have the normalized energy release curve pass through point A thus satisfying the criterion of Eq. (20). For
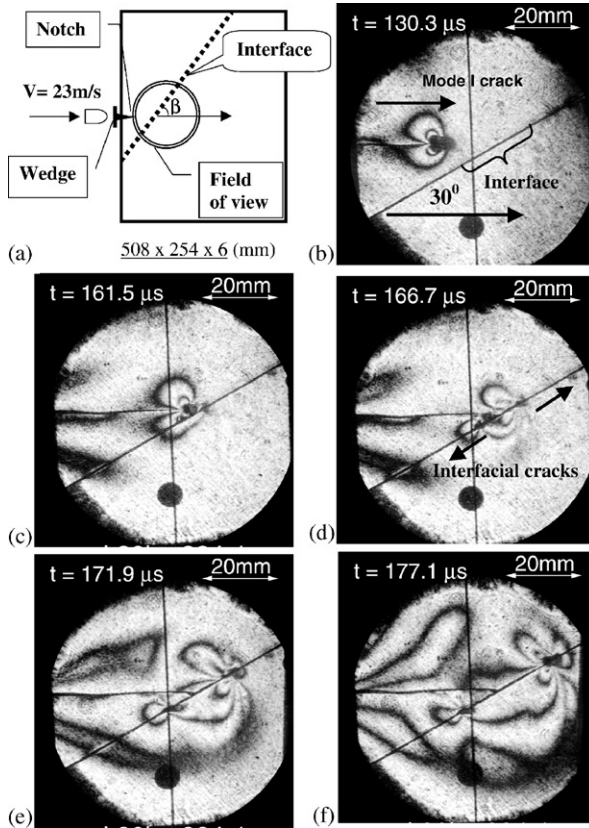
Fig. 18. Remotely induced dynamic interfacial decohesion due to an approaching mode-I crack at a weak interface (interfacial angle 30°).

reference, the curve corresponding to $v_2 = 0$ is also shown. Applying this procedure to the two interface cases discussed in Section 3, we can display the variation of the ratio v_2/v_1 as a function of interfacial angle (see Fig. 17(b)). As expected, the weak interface features higher deflection speeds. Also as the interfacial angle increases, the speed ratio drops in both cases. In particular, for the strong interface case, it drops to zero at an interfacial angle of $\beta = 68°$ beyond which penetration will occur. Table 3 compares these analytical predictions to the observations of interfacial crack tip speeds observed in the experiments described in Section 3. Given the errors in accurate speed estimation just before and after deflection (at least ±100 m/s), the agreement is fairly good.

5.3. Alternative mechanisms of failure mode transition at interfaces

In all cases described above, the incident mode-I crack reached the interface, and within our observation resolution, deflected along it or penetrated through it without nucleating interfacial decohesion at a distance. In Fig. 18, we show an alternative way

of producing failure mode transition which does not fit within our previous discussions but has conceptual similarities. Here a faster incident crack (crack speed is about 450 m/s) races towards a weak interface (Loctite 384 bond) inclined at an angle of 30° to the horizontal. Before the mode-I crack reached the interface (Fig. 18(c)), a central debonding nucleated at the weak interface and started to propagate downwards first and then upwards along the interface. The two crack tips of this debonding clearly had two different speeds as evident from Fig. 18(e) and (f). This phenomenon was observed mainly for specimens featuring weak interfaces and high incident crack speeds (or high stress intensity factor of the incident crack tip) in some of our experiments. It is very reminiscent of the observations displayed in Fig. 1 and discussed in connection to the dynamic "Cook–Gordon mechanism". The static equivalent of this phenomenon was recently analyzed by Arata et al. (2000) and Leguillon et al. (2000) and merits additional attention in the future.

Acknowledgements

References

Ahn, B.K., Curtin, W.A., Parthasarathy, T.A., Dutton, R.E., 1998. Criteria for crack deflection/penetration for fiber-reinforced ceramic matrix composites. Compos. Sci. Technol. 58, 1775–1784.

Anderson, T.L., 1995. Fracture Mechanics, 2nd Edition. CRC Press, Boca Raton, FL.

Arata, J.J.M., Nedleman, A., Kumar, K.S., Curtin, W.A., 2000. Microcrack nucleation and growth in elastic lamellar solids. Int. J. Fract. 105, 321–342.

Broberg, K.B., 1999. Cracks and Fracture. Academic Press, San Diego.

Coker, D., Rosakis, A.J., 2002. Dynamic fracture of unidirectional composite materials: mode-I crack initiation and propagation. Int. J. Fract. submitted.

Cook, J., Gordon, J.E., 1964. A mechanism for the control of crack propagation in all brittle systems. Proc. Roy. Soc. 282A, 508–520.

Cotterell, B., Rice, J.R., 1980. Slightly curved or kinked cracks. Int. J. Fract. 16 (2), 155–169.

Dally, J.W., 1979. Dynamic photoelastic studies of fracture. Exp. Mech. 19, 349–361.

Dienes, J.K., 1996. A unified theory of flow, hot spots, and fragmentation with an application to explosive sensitivity. In: Davison, L. (Ed.), High Pressure Shock Compression of Solids–I. Springer, New York.

Evans, A.G., Zok, F.W., 1994. Review the physics and mechanics of fiber-reinforced brittle matrix composites. J. Mater. Sci. 29, 3857–3896.

Fourney, W.L., Chona, R., Sanford, R.J., 1983. Dynamic crack growth in polymers. In: Knauss, W.G., Ravi-Chandar, K., Rosakis, A.J. (Ed.), Workshop on Dynamic Fracture, Pasadena, Caltech SM Report 83-12, pp.75–99.

Freund, L.B., 1990. Dynamic Fracture Mechanics. Cambridge University Press, New York.

Gao, H., Huang, Y., Gumbsch, P., Rosakis, A.J., 1999. On radiation-free transonicmotion of cracks and dislocations. J. Mech. Phys. Solids 47, 1941–1961.

Geubelle, P.H., Kubair, D., 2001. Intersonic crack propagation in homogeneous media under shear-dominated loading: numerical analysis. J. Mech. Phys. Solids 49, 571–587.

Guduru, P., Zehnder, A.T., Rosakis, A.J., Ravichandran, G., 2001. Dynamic, full-field measurements of crack tip temperatures. Eng. Fract. Mech. 68, 1535–1556.

Gupta, V., Argon, A.S., Suo, Z., 1992. Crack deflection at an interface between two orthotropic materials. J. Appl. Mech. 59, s79–s87.

Hahn, G.T., Hoagland, R.G., Lereim, J., Markworth, A.J., Rosenfield, A.R., 1980. Fast fracture toughness and crack arrest toughness of reactor pressure vessel steel. In: Hanh, G.T.,Kanninen, M.F. (Eds.) Crack arrest methodology and applications, ASTM STP 711, American Society for Testing and Materials, 1980, pp. 289–320.

He, M.Y., Hutchinson, J.W., 1989. Crack deflection at an interface between dissimilar elastic materials. Int. J. Solids Struct. 25, 1053–1067.

He, M.Y., Hsueh, C.H., Becher, P.F., 2000. Deflection versus penetration of a wedge-loaded crack: effects of branch-crack length and penetrated-layer width. Composites: Part B. 31, 299–308.

Hutchinson, J.W., Suo, Z., 1992. Mixed mode cracking in layered materials. Adv. Appl. Mech. 29, 63–191.

Kalthoff, J.F., 1983. On some current problems in experimental fracture. In: Knauss, W.G., Ravi-Chandar, K., Rosakis, A.J. (Eds.), Workshop on Dynamic Fracture, Pasadena, Caltech SM Report 83-12, pp.11–35.

Kobayashi, A.S., Mall, S., 1978. Dynamic fracture toughness of Homalite-100. Exp. Mech. 18, 11–18.

Lambros, J., Rosakis, A.J., 1995. Shear dominated transonic growth in a bimaterial — I. Experimental observations. J. Mech. Phys. Solids 43, 169–188.

Lee, O.S., Knauss, W.G., 1989. Dynamic crack propagation along a weakly bonded planes in a polymer. Exp. Mech. 29, 342–345.

Leguillon, D., Lacroix, C., Martin, E., 2000. Interface debonding ahead of a primary crack. J. Mech. Phys. Solids 48, 2137–2161.

Martinez, D., Gupta, V., 1994. Energy criterion for crack deflection at an interface between two orthotropic media. J. Mech. Phys. Solids. 42 (8), 1247–1271.

Needleman, A., Rosakis, A.J., 1999. The effect of bond strength and loading rate on the conditions governing the attainment of intersonic crack growth along interfaces. J. Mech. Phys. Solids 47, 2411–2449.

Qin, Q.H., Zhang, X., 2000. Crack deflection at an interface between dissimilar piezoelectric materials. Int. J. Fract. 102, 355–370.

Ravi-Chandar, K., Knauss, W.G., 1984. An experimental investigation into dynamic fracture: III on steady-state crack propagation and crack branching. Int. J. Fract. 26, 141–154.

Rosakis, A.J., 2000. Explosion at the Parthenon; can we pick up the pieces? Caltech Solid Mechanics report.

Rosakis, A.J., Ravichandran, G., 2000. Dynamic failure mechanics. Int. J. Solids Struct. 37, 331–348.

Rosakis, A.J., Samudrala, O., Singh, R.P., Shukla, A., 1998. Intersonic crack propagation in bimaterial systems. J. Mech. Phys. Solids 46, 1789–1813.

Rosakis, A.J., Samudrala, O., Coker, D., 1999. Cracks faster than shear wave speed. Science 284, 1337–1340.

Sharon, E., Fineberg, J., 1999. Confirming the continuum theory of dynamic brittle fracture for fast cracks. Nature 397, 333–335.

Siegmund, T., Fleck, N.A., Needleman, A., 1997. Dynamic crack growth across an interface. Int. J. Fract. 85, 381–402.

Thouless, M.D., 1992. Mixed-mode fracture of a lubricated interface. Acta Metall. Mater. 40 (6), 1281–1286.

Washabaugh, P.G., Knauss, W.G., 1994. A reconciliation of dynamic crack growth velocity and Rayleigh wave speed in isotropic brittle solids. Int. J. Fract. 65, 97–114.

Xu, L.R., Rosakis, A.J., 2002a. An experimental study of impact-induced failure events in homogeneous layered materials using dynamic photoelasticity and high-speed photography. Opt. Lasers Eng., in press.

Xu, L.R., Rosakis, A.J., 2002b. Dynamic failure in layered materials with initial defects, in preparation.

Xu, L.R., Rosakis, A.J., 2002c. Impact failure characteristics in sandwich structures; Part II: effects of impact speed and interfacial strength. Int. J. Solids Struct., 39, 4237–4238.

Xu, L.R., Samudrala, O., Rosakis, A.J., 2002. Measurements of Interfacial mechanical properties with the aid of two optical techniques. Proceedings of the 2002 SEM Annual Conference and Exposition on Experimental and Applied Mechanics, Society for Experimental Mechanics, Inc., Bethel, CT, USA, Paper 34.